

ERROR PROPAGATION OF DIRECT PRESSURE GRADIENT INTEGRATION AND A NOVEL PRESSURE FIELD RECONSTRUCTION METHOD BASED ON IMAGE VELOCIMETRY DATA BY HELMHOLTZ-HODGE DECOMPOSITION

Lanyu Li; Jeffrey McClure; Zhao Pan
Dept. Mechanical and Mechatronics Engineering
University of Waterloo, ON N2L 3G1, Canada
lanyu.li; jejmccclu; zhao.pan@uwaterloo.ca

Grady Wright
Dept. Mathematics
Boise State University, Boise, ID 83725, USA
gradywright@boisestate.edu

Jerad P. Whitehead
Mathematics Dept.
Brigham Young University, Provo, UT 84602, USA
whitehead@mathematics.byu.edu

Jin Wang
Independent researcher
3031 NE 137th St Seattle WA 98125, USA
jwang186@jhu.edu

ABSTRACT

Recovering the pressure fields from image velocimetry measurements involves two general strategies: i) direct Pressure Gradient Integration (PGI) from the momentum equation and ii) solving the Pressure Poisson Equation (PPE). In this work, we analyze the error propagation of the former strategy and provide some practical insights. For example, we explain how applying the Helmholtz-Hodge Decomposition (HHD) could significantly reduce the error propagation for the PGI and PPE. We also propose to use a novel Radial Basis Function (RBF)-based HHD pressure field reconstruction strategy that offers the following advantages: i) effective processing of scattered or structured image velocimetry data on a complex domain and ii) divergence/curl-free kernels providing direct divergence-free correction to the velocity fields for incompressible flows and curl-free correction for pressure gradients. Complete elimination of divergence-free bias in measured pressure gradients and curl-free bias in the measured velocity field results in accurate and robust reconstruction. Synthetic Lagrangian particle tracking velocimetry data based on high-fidelity simulations are used to test the analysis, demonstrating the flexibility and effectiveness of the RBF-HHD pressure solver.

INTRODUCTION

Reconstructing pressure fields from image velocimetry is attractive due to its non-invasive nature and field measurement capability. This reconstruction, in general, can be classified into two major categories: i) direct Pressure Gradient Integration (PGI) based on the momentum equation $\nabla p = \mathbf{g}(\mathbf{u}) = -\rho \left(\frac{\partial \mathbf{u}}{\partial t} + (\mathbf{u} \cdot \nabla) \mathbf{u} - \nu \nabla^2 \mathbf{u} \right)$ and ii) solving the Pressure Poisson Equation (PPE), i.e., $\nabla^2 p = f(\mathbf{u}) = \nabla \cdot \nabla p$.

Reconstructing pressure through the PPE and PGI poses different advantages and challenges. One fundamental advantage of solving the PPE is that the reconstructed pressure field is unique (up to a constant reference pressure) given proper boundary conditions, no matter if the data are corrupted or not. However, rigorous error analysis and benchmarking stud-

ies show that solving the PPE could be sensitive to the error in the data (Charonko *et al.*, 2010; Pan *et al.*, 2016). On the other hand, carrying out the PGI along different paths in the domain may give conflicting reconstructed pressure at a fixed location if the pressure gradient data are corrupted. This reflects an ill-posed problem: the uniqueness of the solution is not guaranteed and a regularization technique is needed to address this issue. For example, Baur & Köngeter (1999) integrated pressure gradients starting from an edge of the domain using a spatial-marching strategy. Another typical strategy in the PGI category includes the Omni-Directional Integral (ODI) methods (e.g., the Rotating Parallel Ray Omni-Directional Integration method (RPR-ODI) developed by Liu *et al.* (2016)). The ODI-family algorithms attempt a finite ensemble reconstruction of a pressure field on a discrete mesh. They aim to iteratively impose the Path Independence Property (PIP) of the line integral for a scalar field, whose gradient is supposed to be conservative. Despite the fact that the ODI is robust against random noise in the pressure gradients, its major deficiency is the high computational cost, especially for time-resolved high-resolution volumetric data.

Analyzing the error propagation from the input data to the computed pressure is crucial not only for understanding and improving the reconstruction algorithms but also for uncertainty quantification. The error analysis of the pressure reconstruction based on the PPE has been reported in Pan *et al.* (2016), offering error bounds for the recovered pressure, which are independent of the solver implementations and experimental techniques (e.g., PIV or PTV). Error propagation of the ODI solvers was analyzed by Liu & Moreto (2020), showing that the error in the recovered pressure decreases with the number of integration paths within a certain range when the random noise in the pressure gradient is assumed to be zero-mean. However, rigorous error propagation analysis for the general PGI has not been sufficiently studied yet in the context of image velocimetry-based pressure field reconstruction.

In this work, we attempt such an analysis of the PGI, which leads to several interesting results. First, we show that the continuous limit of the ODI is to apply the Helmholtz-

Hodge Decomposition (HHD) to a measured pressure gradient for regulated pressure reconstruction. Second, a properly conducted PGI could potentially achieve more accurate pressure reconstruction than that recovered by the PPE. Lastly, in lieu of these observations, we propose to use a Radial Basis Function (RBF)-based HHD solver that is based on divergence/curl-free kernels to provide divergence-free correction to the velocity fields for incompressible flows and curl-free correction for pressure gradients, offering the following advantages: i) effective flow reconstruction on scattered PTV data in a complex domain without meshes; ii) detecting and eliminating divergence/curl-free bias in measured data; and iii) significant reduction in computational time compared to conventional ODI methods.

ERROR ESTIMATE FOR PGI (WITH HHD REGULARIZATION)

In this section, we provide an error estimate of the pressure field reconstructed from PGI. Let the uncontaminated pressure gradient be $\mathbf{g} = \nabla p$ in the domain Ω , where p is the pressure field with boundary value $p = p_0$ on $\partial\Omega$. As p is a scalar potential, its gradient \mathbf{g} is a conservative vector field that is curl-free. A fundamental property of a conservative field is that the line integral from one location in the field to the other is independent of the path of the integral, as suggested by the gradient theorem. If ∇p is corrupted by some error $\varepsilon_{\nabla p}$, then we have $\tilde{\mathbf{g}} = \nabla p + \varepsilon_{\nabla p}$ in Ω , and the PIP does not necessarily hold for the contaminated field $\tilde{\mathbf{g}}$, posing difficulty to direct analysis of the error propagation of the PGI. However, this issue could be resolved by applying the HHD on the contaminated pressure field.

One of the formulations of the HHD states that a sufficiently smooth vector field $\boldsymbol{\xi}$ on a bounded domain Ω with boundary $\partial\Omega$ can be *uniquely* decomposed in the form $\boldsymbol{\xi} = \nabla\varphi + \mathbf{r}$, where the vector field \mathbf{r} is divergence-free and is removable. \mathbf{r} is tangential to the boundary along $\partial\Omega$; φ is a scalar potential and $\nabla\varphi$ is curl-free (Chorin *et al.*, 1990). For example, a contaminated pressure gradient field $\tilde{\mathbf{g}}$ can be decomposed as $\tilde{\mathbf{g}} = \nabla p + \varepsilon_{\nabla p} = \nabla\varphi + \mathbf{r}_{\nabla p}$ in Ω . If the conditions on the boundary (e.g., $\hat{\mathbf{n}} \cdot \mathbf{r}_{\nabla p} = 0$) are given, $\hat{\mathbf{n}} \cdot \nabla\varphi = d_n$ is naturally determined. In turn, φ is unique up to a constant, including the value of φ on the boundary: $\varphi = \varphi_0$ on $\partial\Omega$.

The significance of the HHD in the context of pressure reconstruction is that the decomposed gradient field $\nabla\varphi$ *exactly* satisfies the path independence condition for a pressure gradient field and the divergence-free component in $\tilde{\mathbf{g}}$ can be *completely* removed. Note, the outcome of the HHD ($\nabla\varphi$) only guarantees the curl-free property and thus φ is a scalar potential. However, this does not mean that $\nabla\varphi$ is error-free. The HHD only identifies and removes the divergence-free part (i.e., $\mathbf{r}_{\nabla p}$) in $\tilde{\mathbf{g}}$, which should not be there at all.

We next investigate the error ($\varphi - p$) in the reconstructed pressure field when the contaminated field $\tilde{\mathbf{g}}$ is integrated using HHD regularization. Comparing the uncontaminated pressure gradient with the contaminated one, we can isolate the error in the pressure gradient

$$\varepsilon_{\nabla p} = \tilde{\mathbf{g}} - \mathbf{g} = \nabla(\varphi - p) + \mathbf{r}_{\nabla p} \quad \text{in } \Omega, \quad (1)$$

and the discrepancy on the boundary is $\varepsilon_p = \varphi_0 - p_0$ on $\partial\Omega$. Computing the norm of both sides of (1) and applying triangle

inequalities lead to

$$\begin{aligned} \|\varepsilon_{\nabla p}\|_{L^2(\Omega)} &= \|\nabla(\varphi - p) + \mathbf{r}_{\nabla p}\|_{L^2(\Omega)} \\ &\geq \left| \|\nabla(\varphi - p)\|_{L^2(\Omega)} - \|\mathbf{r}_{\nabla p}\|_{L^2(\Omega)} \right| \quad \text{in } \Omega. \end{aligned} \quad (2)$$

Applying the Poincaré inequality to (2), we can bound the discrepancy between the HHD reconstruction and the true value of the pressure:

$$\|\varepsilon_p\|_{L^2(\Omega)} = \|\varphi - p\|_{L^2(\Omega)} \leq C \left(\|\varepsilon_{\nabla p}\|_{L^2(\Omega)} + \|\mathbf{r}_{\nabla p}\|_{L^2(\Omega)} \right), \quad (3)$$

where C is the Poincaré constant. The value of C is independent of the numerical scheme of the pressure solver or experimental method. If the error on the boundary is concerned, the error in the reconstructed pressure field can be bounded as

$$\|\varepsilon_p\|_{L^2(\Omega)} \leq C \left(\|\varepsilon_{\nabla p}\|_{L^2(\Omega)} + \|\mathbf{r}_{\nabla p}\|_{L^2(\Omega)} \right) + \|\varphi_0 - p_0\|_{L^\infty(\partial\Omega)}. \quad (4)$$

HHD-based regularization for improved pressure reconstruction

If a proper HHD is performed to regularize the measured pressure gradient, $\mathbf{r}_{\nabla p}$ is removed from $\tilde{\mathbf{g}}$, and using φ alone to reconstruct the pressure field would reduce the error in the pressure field. The corresponding error estimate can be achieved by removing $\mathbf{r}_{\nabla p}$ in (3) and (4):

$$\|\varepsilon_p\|_{L^2(\Omega)} \leq C \|\varepsilon_{\nabla p}\|_{L^2(\Omega)} \leq C \|\varepsilon_{\nabla p}\|_{L^2(\Omega)} + \|\varphi_0 - p_0\|_{L^\infty(\partial\Omega)}. \quad (5)$$

It is obvious that the estimated error in (5) is potentially lower than that for (4), by a difference of $C\|\mathbf{r}_{\nabla p}\|_{L^2(\Omega)}$. The effectiveness of this simple practice will be demonstrated using an RBF-HHD solver in the next sections. In fact, similar ideas have been pursued from various perspectives to different extents. Examples include the works by Baur & Königter (1999); Liu & Katz (2006); Dabiri *et al.* (2014); Wang *et al.* (2016, 2017); McClure & Yarusevych (2019), and Lin & Xu (2023). The goal shared by these methods is to recover the pressure field from a contaminated pressure gradient field by the endeavor of seeking a curl-free pressure gradient field. These methods fulfilled the goal at different levels of success.

HHD-regularized PGI as a limit of ODI

The goal of the ODI is to recover a pressure field aiming to satisfy the PIP of the pressure gradient. Invoking the curl-free property of $\nabla\varphi$ from the HHD, which *exactly* satisfies the PIP, we can argue that the limit of applying the ODI on a corrupted pressure gradient field is carrying out the HHD-based regularization to the same field. If it is possible to find a bound for the error in the pressure computed by the ODI, it is expected to be higher than that in (5).

In addition, the ODI family methods may present some fundamental features that extend beyond the potentially high computational cost, which may have become a minor concern with recent improvements in computational efficiency (Zigunov & Charonko, 2023, 2024): i) the ODI cannot differentiate the curl-free error in the pressure gradient, as the curl-free error also satisfies the PIP. This is the same as the HHD-based pressure solvers. Thus, such errors in the pressure gradient can penetrate through reconstruction, by either

the ODI family or HHD-based methods, and contaminate the recovered pressure field; ii) the ODI does not necessarily reject any divergence-free components in the pressure gradient (i.e., $\mathbf{r}_{\nabla p}$), while the divergence-free error could be removed by the HHD-based methods. Recent advancement of the ODI (Zigunov & Charonko, 2023, 2024) showed that the ODI family has close connections to the PPE. Despite that the original motivation of the ODI algorithm is to iteratively converge to a pressure field whose gradient satisfies the PIP, the simplification by Zigunov & Charonko (2024) does not show the curl-free correction intended by the ODI.

Connections between PPE and HHD-regularized PGI

Assuming $\mathbf{r}_{\nabla p}$ is small or removable, ignoring $\|\mathbf{r}_{\nabla p}\|_{L^2(\Omega)}$ in (3) leads to $\|\varphi - p\|_{L^2(\Omega)} \leq C\|\varepsilon_{\nabla p}\|_{L^2(\Omega)}$. More explicitly, this assumption implies that only the curl-free part of $\varepsilon_{\nabla p}$ is relevant for error propagation. This means that $\varepsilon_{\nabla p} = \nabla \varepsilon_p$ and $\varepsilon_p = \varphi - p$, and we can obtain

$$\|\varepsilon_p\|_{L^2(\Omega)} \leq C\|\nabla \varepsilon_p\|_{L^2(\Omega)}. \quad (6)$$

Recalling the error estimate of the PPE which is based on the analysis of the Poisson equation with respect to ε_p (details can be found in Pan *et al.* (2016)): $\nabla^2 \varepsilon_p = \nabla \cdot \nabla \varepsilon_p = \varepsilon_f$, where ε_f is the error in the data of the PPE, we can apply the Poincaré inequality which leads to

$$\|\nabla \varepsilon_p\|_{L^2(\Omega)} \leq C\|\varepsilon_f\|_{L^2(\Omega)}. \quad (7)$$

Combining (6) and (7) recovers the error bound by directly analyzing the PPE:

$$\|\varepsilon_p\|_{L^2(\Omega)} \leq \underbrace{C\|\varepsilon_{\nabla p}\|_{L^2(\Omega)}}_{\text{bound for HHD}} \approx C\|\nabla \varepsilon_p\|_{L^2(\Omega)} \leq \underbrace{C^2\|\varepsilon_f\|_{L^2(\Omega)}}_{\text{bound for PPE}}. \quad (8)$$

The error estimation (8) recovers the heuristic that an HHD-regularized PGI solver is expected to outperform a normal Poisson solver in terms of upper bounds. However, in reality, a direct comparison between these two strategies is not trivial for several reasons. First, for example, using the Poincaré inequality twice (i.e., C^2 in (8)) for a PPE-based solver may overestimate the error in the pressure reconstruction more significantly than the error estimate for an HHD-based solver, where the Poincaré inequality is applied only once. Second, the bound for the HHD-based solver scales with the error in the pressure gradient $\|\varepsilon_{\nabla p}\|_{L^2(\Omega)}$ but the bound for the PPE-based solver scales with the error in the data field $\|\varepsilon_f\|_{L^2(\Omega)}$. The relative value of $\varepsilon_{\nabla p}$ and ε_f is not straightforward, in addition to the complexity associated with numerical implementation when evaluating these quantities. One simple example demonstrating this issue can be found in Nie *et al.* (2022).

AN RBF-HHD SOLVER

In this work, we employ an RBF-HHD solver developed by Fuselier & Wright (2017) to reconstruct the pressure field. The use of this solver serves two purposes: i) validate some of the arguments in the previous sections, and ii) demonstrate the effectiveness of this solver as a novel pressure field reconstruction method suitable for contaminated image velocimetry data.

The general idea behind the RBF-HHD solver is summarized below, and details can be found in Fuselier & Wright (2017). A generalized matrix-valued RBF kernel Φ can be decomposed into a divergence-free and curl-free part on a bounded domain: $\Phi = \Phi^{\text{df}} + \Phi^{\text{cf}}$, where $\Phi^{\text{df}} = -\mathbf{curl}_x \mathbf{curl}_y (\phi(|x-y|)\mathbf{I})$ and $\Phi^{\text{cf}} = \nabla_x \nabla_y^T (\phi(|x-y|)\mathbf{I})$ are the divergence-free and curl-free kernels, respectively. \mathbf{curl} and ∇ are the curl and gradient operators, respectively, and their subscript (e.g., the x in \mathbf{curl}_x or the y in ∇_y) denotes the argument it acts on; \mathbf{I} is an identity matrix. $\phi(|x-y|)$ represents an RBF kernel, which is the scalar-valued form of Φ . x and y are two data points in the domain and $|x-y|$ denotes their Euclidean distance. The superscript $[\cdot]^T$ denotes the matrix transpose operator. This decomposition is unique and the construction of the divergence-free and curl-free kernels for 2D or 3D is straightforward.

Using the kernels Φ^{df} and Φ^{cf} , a vector field \mathbf{s}_f can be decomposed into divergence-free and curl-free parts, i.e., $\mathbf{s}_f = \mathbf{s}_f^{\text{df}} + \mathbf{s}_f^{\text{cf}}$. The decomposed part is a linear combination of Φ^{df} or Φ^{cf} , weighted by a generalized expansion coefficients λ_j . It can be represented by $\mathbf{s}_f^{\text{df}} = \sum_{j=1}^N \Phi^{\text{df}}(\cdot, x_j) \lambda_j$ and $\mathbf{s}_f^{\text{cf}} = \sum_{j=1}^N \Phi^{\text{cf}}(\cdot, x_j) \lambda_j$, where x_j is the location of the given data point, N is the number of given data points. The expansion coefficients λ_j can be solved by forcing the interpolant coinciding with the given data $\mathbf{f}|_X$: $\mathbf{s}_f|_X = \mathbf{f}|_X = \sum_{j=1}^N \Phi(X, x_j) \lambda_j$, where $X = \{x_1, x_2, \dots, x_N\}$ represents the locations of the given data. After retrieving λ_j , we can obtain the decomposed divergence-free and curl-free parts.

The divergence-free RBF-HHD solver for velocity field reconstruction and the curl-free RBF-HHD solver for pressure field reconstruction are constructed based on the above decomposition. When solving λ_j , the divergence-free solver utilizes Φ^{df} ; and its boundary conditions are prescribed as the outward normal components of vectors at boundaries in the divergence-free part. On the other hand, the curl-free solver employs Φ^{cf} ; and its boundary conditions require the tangential components of vectors at boundaries in the curl-free part. After the decomposition, the divergence-free RBF-HHD velocity solver removes the curl-free bias in the velocity field for an incompressible flow. The curl-free RBF-HHD pressure solver filters out the divergence-free component in the pressure gradients and calculates the potential of the pressure gradients (i.e., the pressure field). The potential is evaluated by a linear combination of kernels $-\nabla_y^T (\phi(|x-y|))$, whose coefficients are known from the previous step.

VALIDATION: A 2D LAMINAR CYLINDER FLOW

A two-dimensional, laminar, uniform flow around a circular cylinder for a Reynolds number $Re = 100$ is used to showcase the RBF-HHD solvers and demonstrate some of the arguments in the previous sections.

We first use a high-fidelity simulation to generate the ground truth of the flow field. The free stream velocity of the flow is $U_\infty = 1$, the kinematic viscosity is $\nu = 0.01$, and the density is $\rho = 1$. The numerical simulation domain spans from $(x/D, y/D) = [-8, 25] \times [-8, 8]$. The boundary conditions for the simulation are a uniform stream-wise velocity inlet at $x/D = -8$, a pressure outlet $p = 0$ at $x/D = 25$, symmetry planes at $y/D = \pm 8$, and a non-slip wall at the cylinder. We use a structured mesh with about 0.75 million cells to discretize the simulation domain, with mesh refinement near the cylinder and wake region.

The validation is performed within a rectangular recon-

struction domain cropped from the simulation domain, as depicted in Fig. 1(a). The reconstruction domain encloses the stagnation region in front of the cylinder and the oscillating wake behind it. The center of the cylinder with diameter $D = 1$ is placed at $(x/D, y/D) = (0, 0)$. The reconstruction domain spans $(x/D, y/D) = [-1, 3] \times [-1, 1]$. We use U_∞ , D , and $P_\infty = \frac{1}{2}\rho U_\infty^2$ as the characteristic scales to normalize the velocity, pressure, and pressure gradients, respectively, as well as the corresponding reconstruction errors.

To emulate realistic PTV experiments, synthetic Lagrangian data were generated by imposing Gaussian noise on the true value of the velocity sampled at pseudo-particles in the domain. About 1.1×10^4 pathlines originated at random and unique locations are generated in the domain. These pathlines are computed by integrating the interpolated instantaneous velocity. The velocity and pressure at the particle locations along the pathlines are interpolated using the data from the simulation, serving as the ground truth for validation. Lastly, we impose zero-mean Gaussian noise on the particle velocity. This artificially corrupted velocity field is used as the synthetic PTV data. The standard deviation of the artificial noise is equal to 1% of the magnitude of the local velocity.

To reconstruct the pressure fields from the velocity fields, we evaluate the pressure gradients from the synthetic Lagrangian data first, and then the pressure fields are computed based on these pressure gradients. The material acceleration in the pressure gradient was evaluated by approximating the velocity change when following a particle along its pathline (Van Oudheusden, 2013). The viscous term in the pressure gradient is computed using the least squares RBF-QR algorithm (Fornberg *et al.*, 2011; Larsson *et al.*, 2013).

Note that before computing the pressure gradients, we have the option to filter out the curl-free part of the corrupted velocity field using the divergence-free RBF-HHD velocity solver. We refer to this option as the velocity correction, which can improve the final reconstruction accuracy. The tangential components of the velocities at boundaries in the divergence-free part can be easily obtained by interpolating the velocimetry data.

After recovering the pressure gradients, we use the curl-free RBF-HHD solver to reconstruct the pressure fields. For this pressure solver, we specify the tangential components of the pressure gradients at boundaries in the curl-free part, which are parallel to the boundaries. 500 independent tests were carried out for the validation. We compute a space-averaged L^2 -norm of the error to assess reconstruction quality: $\|\epsilon\|_{L^2(\Omega)} = \sqrt{(\int \epsilon^2 d\Omega)/\Omega}$, where ϵ represents the absolute error between the reconstructed results and the ground truth.

Typical results of reconstruction and error statistics are presented in Figs. 1 – 3. Figure 1 illustrates the true value of the velocity, vorticity, and pressure fields as references, as well as the synthetic velocimetry data (c1) and the corrected velocity field (c2). The curl-free component (d) is extracted from the contaminated velocity field (c1) and we obtain the divergence-free velocity field (c2).

Figure 2 illustrates the pressure gradients (a1) – (a2) and reconstructed pressure fields (c1) – (c2) using the curl-free RBF-HHD pressure solver. The left and right columns in Fig. 2 are the results based on the velocity field without and with divergence-free correction, respectively. The removed divergence-free error in the pressure gradient is shown (b1) – (b2). For this particular flow, the divergence-free error in the pressure field peaks near the stagnation region of the flow. This is perhaps due to intrinsically high pressure gradients and relatively low particle density near the wall that conflicts the

boundary condition of the curl-free RBF-HHD pressure solver. Nevertheless, as shown in (c1) – (c2), the reconstructed pressure fields were similar to the ground truth (see Fig. 1(b)), even if the pressure gradients were contaminated.

The errors in the reconstructed pressure gradients and pressure fields are shown in Fig 3. When the divergence-free correction is not applied to the velocity field, the mean error in the reconstructed pressure field is about 4.5% (red box in (b1)), despite a higher error of 29.5% persisting in the pressure gradients (red box in (a1)), which is used as the input to the curl-free RBF-HHD pressure solver. This indicates that the curl-free RBF-HHD solver is robust to the noise in the data. If the divergence-free velocity correction is employed, the errors in reconstructed pressure gradients and pressure field can be reduced to about 8% (blue box in (a1)). This error reduction is evident by comparing the error field of the pressure gradient in (a2) and (a3). The curl-free RBF-HHD pressure solver finally leads to a pressure reconstruction with a mean error level of 3.8%. This demonstrates that the divergence-free RBF-HHD can further improve the pressure reconstruction.

CONCLUSIONS

In this study, we conduct an error propagation analysis concerning the general Pressure Gradient Integration (PGI). Our analysis yields several findings regarding error propagation. First, we show that applying the HHD-regularization on a corrupted pressure gradient field can significantly reduce the error in the reconstructed pressure. The HHD can uniquely decompose a corrupted pressure gradient field into curl-free, which satisfies the path independence property (PIP) of a pressure gradient field, and a divergence-free part, which should not be in the pressure gradient at all. If we remove the divergence-free part and reconstruct the pressure field solely based on the curl-free part of the corrupted pressure gradient, accurate pressure reconstruction is expected.

Second, we argue that the HHD-regularized PGI is a continuous limit of the ODI. While the ODI endeavors to satisfy the PIP, the HHD-regularized PGI can precisely recover a pressure field from a corrected pressure gradient that guarantees the PIP.

Third, the error analysis connects the error propagation for the PPE and HHD-regularized PGI. We suggest that the HHD-regularized PGI can potentially outperform the PPE since the HHD-regularized PGI has a lower upper bound than that of the PPE, which is rooted in integration twice or once to obtain the pressure from $\nabla^2 p = f$ and $\nabla p = \mathbf{g}$, respectively.

Lastly, we propose to use RBF-HHD solvers that are based on divergence/curl-free kernels to provide divergence-free correction to the velocity fields for incompressible flows and curl-free correction for pressure gradients. These solvers can also reconstruct pressure fields from pressure gradients, offering the following advantages: i) flexible computation on scattered and/or structured data on a complex domain without requiring Dirichlet BCs except for a reference pressure, and ii) complete elimination of divergence/curl-free bias in measured data, resulting in accurate and robust pressure reconstruction. Validation based on synthetic PTV data of a 2D laminar cylinder flow demonstrated the competence of the proposed solvers.

ACKNOWLEDGMENT

We thank the Digital Research Alliances of Canada for providing high-performance computing resources. L.L. is par-

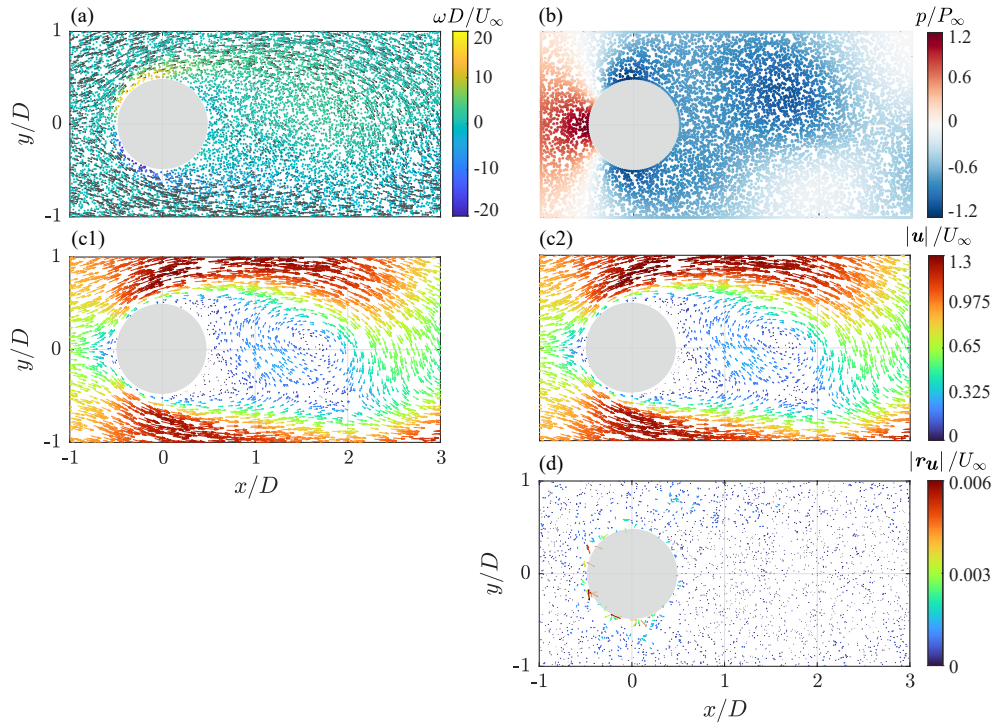


Figure 1. The ground truth of the flow field (a) quiver plot of the velocity field overlaid on the vorticity field, (b) the pressure field; (c1&2) corrupted velocity fields before and after divergence-free correction, respectively; (d) the curl-free components removed from the velocity field (c1) by the divergence-free RBF-HHD solver.

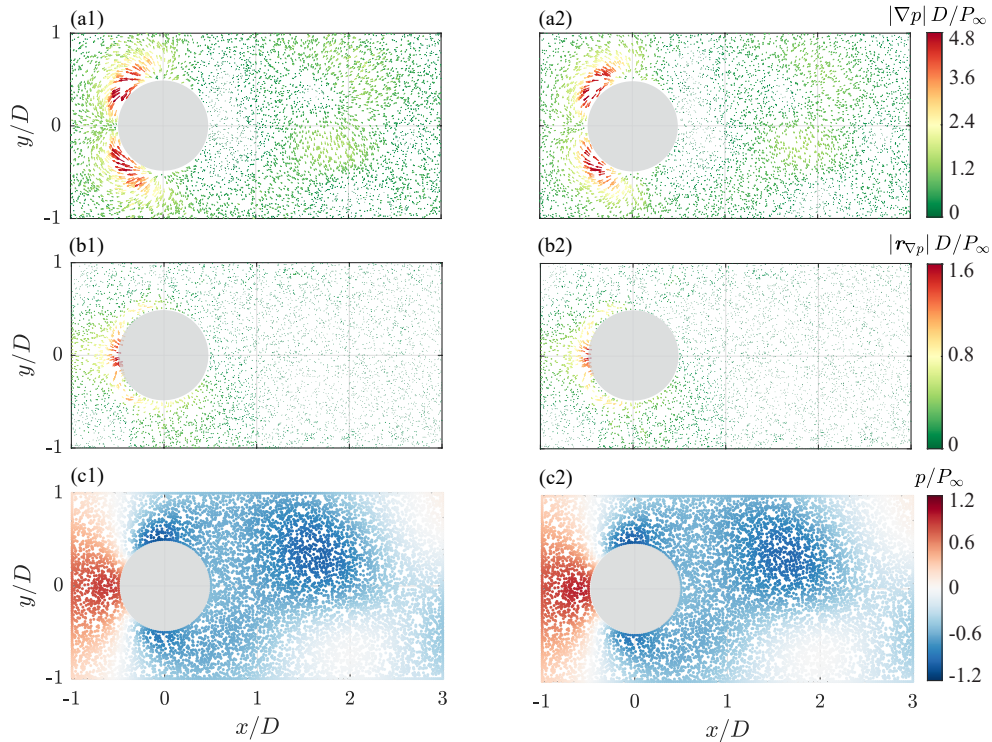


Figure 2. Reconstructed pressure gradients and the pressure field. (a1&2) pressure gradient fields, computed from Fig. 1(c1) and (c2), respectively. (b1&2) the divergence-free parts in the pressure gradients of (a1&2), respectively, identified by the curl-free RBF-HHD pressure solver. (c1&2) reconstructed pressure fields after (b1&2) are removed from (a1&2).

tially supported by the Natural Sciences and Engineering Research Council of Canada (NSERC) Discovery Grant (RGPIN-2020-04486). G.B.W was partially supported by NSF grant DMS-1952674. J.P.W. was partially supported by NSF grant

DMS-2206762.

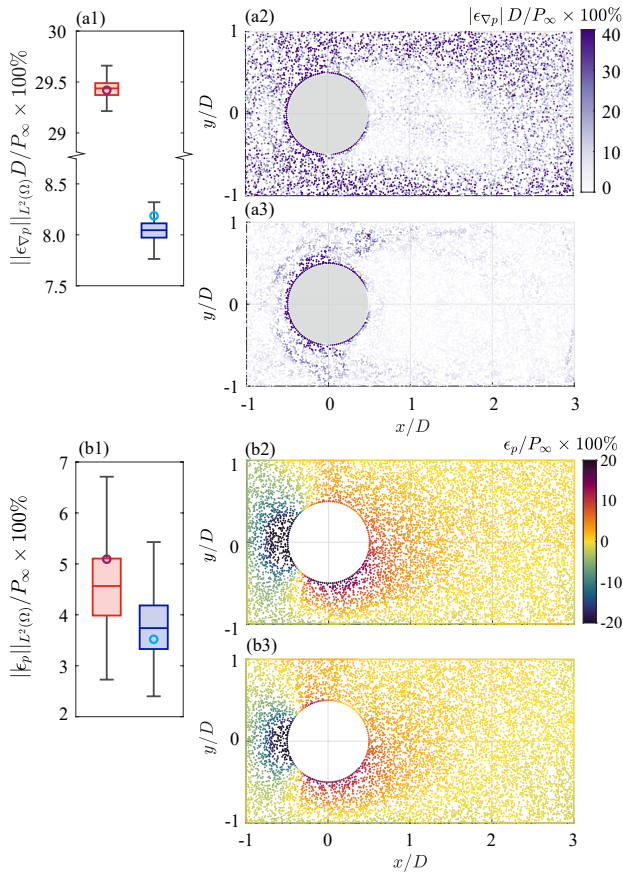


Figure 3. Statistics and typical results for the error in the pressure gradient and pressure fields. A box plot of the error in the reconstructed pressure gradient (a1) and pressure (b1) from 500 independent tests with the red and blue boxes corresponding to the statistics of the error without and with the velocity correction, respectively. Horizontal bars in the middle of the boxes show the median while the upper and lower edges of the box indicate the 25 and 75 percentiles. The upper and lower whiskers bound the 95% confidence intervals of the error. The symbols within the boxes mark where the corresponding error is shown in (a2&3) for the reconstructed pressure gradients; and in (b2&3) for the reconstructed pressure field. (a2&b2) and (a3&b3) are error fields based on the reconstruction without and with the velocity correction, respectively.

REFERENCES

Baur, T & Köngeter, J 1999 PIV with high temporal resolution for the determination of local pressure reductions from coherent turbulence phenomena. In *International Workshop on PIV'99- Santa Barbara, 3rd, Santa Barbara, CA*, pp. 101–106.

Charonko, John J, King, Cameron V, Smith, Barton L & Vlachos, Pavlos P 2010 Assessment of pressure field calculations from particle image velocimetry measurements. *Meas. Sci. Technol.* **21** (10), 105401.

Chorin, Alexandre Joel, Marsden, Jerrold E & Marsden, Jerrold E 1990 *A mathematical introduction to fluid mechanics*, vol. 3. Springer.

Dabiri, John O., Bose, Sanjeeb, Gemmell, Brad J., Colin, Sean P. & Costello, John H. 2014 An algorithm to estimate unsteady and quasi-steady pressure fields from velocity field measurements. *Journal of Experimental Biology* **217** (3), 331–336.

Fornberg, Bengt, Larsson, Elisabeth & Flyer, Natasha 2011 Stable computations with gaussian radial basis functions. *SIAM Journal on Scientific Computing* **33** (2), 869–892.

Fuselier, Edward J & Wright, Grady B 2017 A radial basis function method for computing Helmholtz–Hodge decompositions. *IMA J. Numer. Anal.* **37** (2), 774–797.

Larsson, Elisabeth, Lehto, Erik, Heryudono, Alfa & Fornberg, Bengt 2013 Stable computation of differentiation matrices and scattered node stencils based on Gaussian radial basis functions. *SIAM Journal on Scientific Computing* **35** (4), A2096–A2119.

Lin, Yuhe & Xu, Haitao 2023 Divergence–curl correction for pressure field reconstruction from acceleration in turbulent flows. *Experiments in Fluids* **64** (137).

Liu, Xiaofeng & Katz, Joseph 2006 Instantaneous pressure and material acceleration measurements using a four-exposure PIV system. *Experiments in Fluids* **41** (2), 227–240.

Liu, Xiaofeng & Moreto, Jose Roberto 2020 Error propagation from the PIV-based pressure gradient to the integrated pressure by the omnidirectional integration method. *Meas. Sci. Technol.* **31** (5), 055301.

Liu, Xiaofeng, Moreto, Jose R & Siddle-Mitchell, Seth 2016 Instantaneous pressure reconstruction from measured pressure gradient using rotating parallel ray method. In *54th AIAA Aerospace Sciences Meeting*, p. 1049.

McClure, Jeffrey & Yarusevych, Serhiy 2019 Generalized framework for PIV-based pressure gradient error field determination and correction. *Measurement Science and Technology* **30** (8), 084005.

Nie, Mingyuan, Whitehead, Jared P., Richards, Geordie, Smith, Barton L. & Pan, Zhao 2022 Error propagation dynamics of PIV-based pressure field calculation (3): what is the minimum resolvable pressure in a reconstructed field? *Experiments in Fluids* **63** (11), 168.

Pan, Zhao, Whitehead, Jared, Thomson, Scott & Truscott, Tadd 2016 Error propagation dynamics of PIV-based pressure field calculations: How well does the pressure Poisson solver perform inherently? *Measurement Science and Technology* **27** (8), 084012.

Van Oudheusden, BW 2013 PIV-based pressure measurement. *Measurement Science and Technology* **24** (3), 032001.

Wang, ChengYue, Gao, Qi, Wei, RunJie, Li, Tian & Wang, JinJun 2017 Weighted divergence correction scheme and its fast implementation. *Exp. Fluids* **58**, 1–14.

Wang, Zhongyi, Gao, Qi, Wang, Chengyue, Wei, Runjie & Wang, Jinjun 2016 An irrotation correction on pressure gradient and orthogonal-path integration for PIV-based pressure reconstruction. *Exp. Fluids* **57**, 1–16.

Zigunov, Fernando & Charonko, John 2023 A fast, matrix-based method to perform omnidirectional pressure integration. *Measurement Science and Technology*.

Zigunov, Fernando & Charonko, John 2024 One-shot omnidirectional pressure integration through matrix inversion. *arXiv preprint arXiv:2402.09988*.